Next Materials 13 (2026) 102641

Contents lists available at ScienceDirect

Next Materials

journal homepage: www.sciencedirect.com/journal/next-materials

Research article

Deep learning-based surrogate model for generation of wood microstructures

Marcin Mińkowski [a],*, Fahime Seyedheydari [a], Mikko Seppi [b], Bin Chen [c], Davide Grassano [d], Simo Särkkä [a,e]

[a] Department of Electrical Engineering and Automation, Aalto University, Espoo, Finland
[b] VTT Technical Research Centre of Finland Ltd., P.O. Box 1000, FI-02044 VTT, Espoo, Finland
[c] KTH Royal Institute of Technology, Department of Fibre and Polymer Technology, Wallenberg Science Center, SE-10044, Stockholm, Sweden
[d] Centre Européen de Calcul Atomique et Moléculaire (CECAM), Ecole Polytechnique Fédérale de Lausanne, CH-1015, Lausanne, Switzerland
[e] ELLIS Institute Finland, Espoo, Finland

ARTICLE INFO

Dataset link: https://github.com/MarcinMinkowski/wood-microstructure-surrogate/tree/main/wood-microstructure, https://github.com/AI-TranspWood/AITW_microstructures

Keywords:
Multiphase composites
Material modeling
Transfer learning

ABSTRACT

A machine learning-based surrogate model for efficient wood microstructure generation compatible with a physics-based model is developed. The model is based on the U-Net neural network, a variant of convolutional neural network which, due to its architecture, is suitable for image-to-image transformation, and focuses on the crucial step of the microstructure generation, which is distortion of the wood slices according to the prescribed distortion map. For training the U-Net, a dataset consisting of a variety of wood microstructures slices before and after the distortion is generated, along with the corresponding distortion maps, using the previously developed parametric model. Transfer learning is shown to improve the performance of the U-Net, especially if the dataset of wood slices is small. The best results with transfer learning are obtained if either the whole U-Net is fine-tuned or only the bottleneck block is frozen during the fine-tuning. The surrogate model is a promising tool for generating a large dataset of wood microstructures within the structural parameter ranges it was trained on in a relatively short time compared to the original method. That could in turn be useful for a parametric study and optimization of the physical properties of wood-based materials.

1. Introduction

Predicting physical properties, such as mechanical [1], optical [2] or thermal [3] properties of a material based on its structure and composition, is one of the most important goals in material design and discovery [4–8]. Integrating several phases in the material microstructure, which results in a structure known as a composite material, can lead to a wide variety of those properties [9,10]. An example of a multiphase composite with interesting physical properties is transparent wood biocomposites. First discovered in 1992 by Siegfried Fink [11] and rediscovered more than 20 years later by the research groups of Lars Berglund [12] and Liangbing Hu [13], transparent wood composites exhibit optical transmittance as high as 90% and mechanical strength as high as 270 MPa [12–15]. Owing to these properties, combined with being sustainable, renewable, and biodegradable, transparent wood is considered a potential replacement for commonly used materials, such as plastic or glass [16–19].

Modeling of wood-based materials is generally a challenging task due to their complex morphology resulting from the combination of three-dimensional fibers, vessels, and ray cells, which are structures typically observed in wood [20–22]. Moreover, the growth of fibers and vessels distorts the structure of neighboring cells. Taking this distortion into account is another challenge in modeling realistic wood microstructures. The available models usually simulate two-dimensional microstructures based on scanning electron microscopy (SEM) images and subsequently extend them along the longitudinal dimension. Such models have been used in studies of light propagation [23,24], light absorption [25], mechanical properties [26], heat transfer [27,28], and mass transfer in biomass [29]. They, however, have their limitations since they do not take into account the existence of ray cells and the variation of the microstructure in the longitudinal direction.

Recently, a three-dimensional distortion-map-based model capable of generating such realistic wood microstructures with all the necessary details has been developed [30]. Using this model, a single three-dimensional wood sample is built by first generating a backbone microstructure of fibers, vessels, and ray cells, followed by distorting it using volume image interpolation with a specifically designed distortion map. It is a parametric model that can accurately reproduce the complex wood microstructure comprising the fibers, vessels and ray cells. It shows an accurate description of the wood microstructural complexity when compared to the microscopy images. This advanced model

* Corresponding author.
E-mail address: marcin.minkowski@aalto.fi (M. Mińkowski).

https://doi.org/10.1016/j.nxmate.2026.102641
Received 20 February 2026; Received in revised form 16 June 2026; Accepted 26 June 2026
Available online 4 August 2026

has great potential in predicting the physical properties (e.g., optical and mechanical) of wood-based composites, such as transparent wood.

The aforementioned method can numerically generate a large variety of high-fidelity three-dimensional wood microstructures by adjusting the key microstructural parameters, such as fiber size, fiber length, or cell wall thickness. The generated data can be subsequently used for the parametric study of the physical properties of wood. The model has been applied to study light scattering in transparent wood using the ray tracing technique [31]. However, creating a single three-dimensional wood microstructure using the distortion-map-based model is computationally expensive, making the generation of a whole dataset not practical. The distortion of wood microstructures within this model is the most time-consuming step. Currently, there is no surrogate model that can accurately and efficiently replicate this distortion process. This motivates the development of a fast and reliable machine learning (ML)-based approach for that specific step in the generation of the wood microstructure.

The recent advancement of ML technologies has been helpful in many fields of science and technology. In the field of materials science, ML has been applied in the design, analysis, and prediction of materials properties [32–34]. For instance, convolutional neural networks (CNNs) have been useful in the prediction and optimization of mechanical properties [35,36], feature extraction [37,38], and pattern recognition [39,40].

A particular variant of CNN, U-Net, was originally developed for biomedical image segmentation [41]. U-Net has achieved state-of-the-art results on several biomedical segmentation challenges, substantially outperforming previous methods in tasks such as neuronal structure segmentation and cell tracking [41–43]. Its architecture, consisting of a contracting path followed by an expanding one, also makes it suitable for various image-to-image translation problems such as de-noising and de-blurring of images [44,45], cone-beam computed tomography [46–48], road extraction [49,50], or infrared small object detection [51,52]. The U-Net has also been applied for image restoration for object distortion [53–55]. A related problem, distortion of the image according to the prescribed distortion map is the subject of this work.

Transfer learning aims to improve the performance of an ML model in a target domain by utilizing knowledge from a related source domain, especially when obtaining sufficient labeled data in the target domain is difficult or expensive [56]. Surveys of transfer learning techniques highlight their applications across domains such as text classification and image recognition, and discuss their suitability for big data environments [57]. In deep learning, particularly with CNNs, early layers capture general features such as edges and textures that are transferable across domains, therefore the trainable parameters corresponding to those layers often remain frozen during the fine-tuning of the network. Transfer learning reduces training time, lowers data requirements, and improves model generalization, particularly when labeled data is scarce [58].

Recent work demonstrates that integrating transfer learning with U-Net architectures significantly enhances performance in medical image segmentation tasks [59–61]. By leveraging pre-trained encoders, such as VGG16, these models improve feature extraction and segmentation accuracy, particularly in domains with limited annotated data [62,63].

The contribution of this work is to develop an ML-based surrogate model to speed up generation of wood microstructures compatible with those generated by the parametric model developed earlier [30]. The model focuses on the crucial step of the wood microstructure generation, which is distortion of the slices of wood microstructures, and is based on a U-Net neural network, which is trained to distort an input image according to the prescribed distortion map. Transfer learning is implemented to improve the performance of the U-Net on the wood microstructures by first pre-training it on randomly generated images before fine-tuning it on the wood structures. We test the effect of freezing different training parameters during fine-tuning of the network on the final result. It is shown that for certain freezing schemes, transfer learning outperforms training the network from scratch.

The manuscript is organized as follows. In Section 2, the original distortion-map-based model for wood microstructure generation is recalled and described briefly, and the method of generating the dataset with this model is described; in Section 3, the architecture of the surrogate model is presented, and its training procedure is described; in Section 4, the predictions of the surrogate model are shown and compared with the original model; finally, in Section 5, the results of the work are summarized and concluded.

2. Wood microstructure dataset generation

In this section, the main features of the distortion-map-based model of generating three-dimensional wood microstructures [30] are recalled. It is also discussed how constructing a surrogate model for the local distortion will improve the efficiency of the original model. A method for generating a dataset for training the surrogate model is also described in this section.

2.1. Distortion-map-based method of generating 3D wood microstructures

The distortion-map-based model for realistic 3D wood microstructure generation was proposed [30] and implemented as a MATLAB code. It is a parametric model with many structural parameters (such as fiber size, fiber length, existence of ray cells, vessels, cell wall thickness) of the desired wood microstructures given as input to the code. Here, we briefly recall the main features of the model.

The structure generation in the distortion-map-based model [30] proceeds in several steps: generation of a backbone structure, generation of local and global distortion maps, and distorting the backbone microstructure according to those maps. In each step the output representing the slices of the obtained structure is stored as grayscale image files. The backbone structure has a very regular geometry with typical ellipsoidal fibers extended along the tree growth (longitudinal) direction, and ray cells pointing from the trunk center to peels (radial direction). The generation of local and global distortion maps aims to mimic the physiological function of fiber growth in wood. Applying the distortion map to the backbone structure can generate a high-fidelity microstructure. The final output of the model is a 3D wood microstructure, an example of which is shown in Fig. 1.

In the first step of the algorithm, sparse slices are constructed by fitting elliptical cross-sections of fibers and vessels to nodes arranged in a square grid with some added random disturbance. The fibers are hexagonally distributed throughout the slice, while positions of the vessels are chosen randomly. Additionally, at random positions, white strips elongated in the radial direction are inserted, which are later filled with ray cells. The sparse slices are then interpolated along the longitudinal direction, creating a three-dimensional backbone structure.

In the next step, local distortion of the backbone structure is performed. Its purpose is to imitate the effect of the growth of fibers and vessels on neighboring cells. The map for the local distortion is given as

$$u_{li}\left(\mathbf{x},\mathbf{k},\mathbf{x_c}\right) = w\left(y\right) u_0\left(x\right), \tag{1}$$

with

$$u_0\left(x\right) = \left[\frac{1}{1+e^{-k_1(x-x_c)}} - \frac{1}{1+e^{-k_2(x-x_c)}}\right], \tag{2}$$

$$w\left(y\right) = \frac{k_4}{k_2} e^{-\frac{(y-y_c)^2}{2(k_3/k_2)^2}}, \tag{3}$$

where u_{li} is the local distortion field at the point $\mathbf{x} = (x, y)$ in the space produced by an individual fiber or vessel centered at $\mathbf{x_c} = (x_c, y_c)$ and $\mathbf{k} = (k_1, k_2, k_3, k_4)$ are parameters of the distortion. For each slice, the local distortion is summed up over all the fibers and vessels. The effect

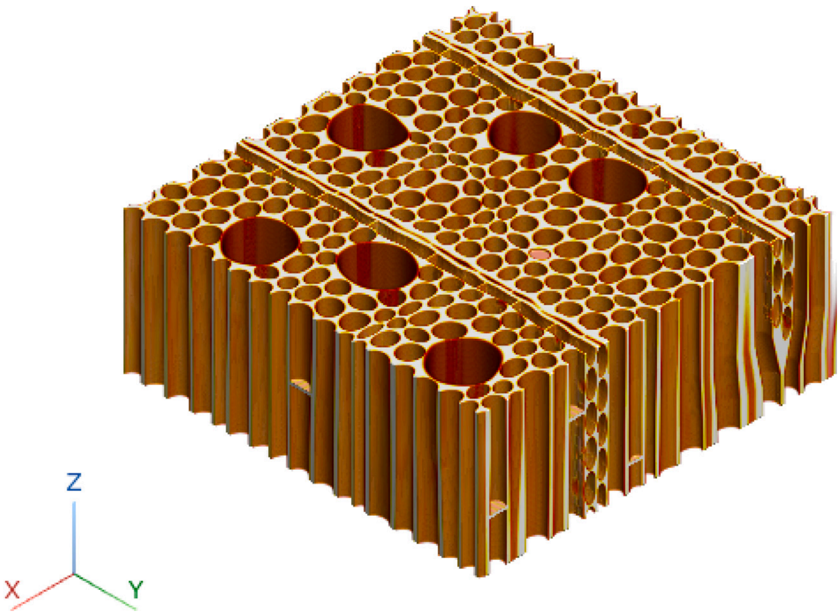

Fig. 1. A 3D birch microstructure containing fibers, vessels and ray cells generated with the method developed in the paper [30]. The x-axis is oriented along the tangential direction of the wood microstructure, y-axis along the radial direction and z-axis along the longitudinal direction.

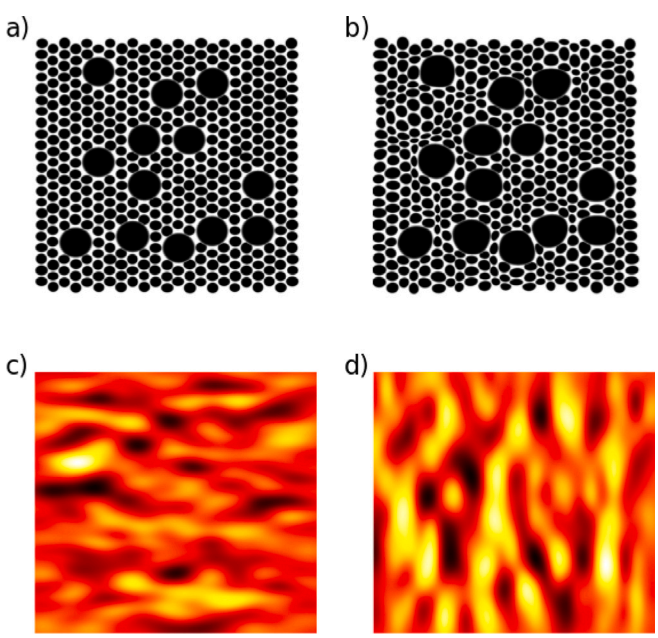

Fig. 2. A single slice of a sample wood microstructure generated by the distortion-map-based model: (a) before distortion, (b) after distortion, (c) u-element of the distortion map, (d) w-element of the distortion map.

of local distortion on a single slice of birch microstructure, along with the corresponding distortion maps, is demonstrated in Fig. 2.

The local distortion is followed by the global distortion, which involves distorting the fiber groups and twisting the whole structure. It results in the final structure as seen in Fig. 1. As already discussed in the paper [30] it can be observed there that the resulting structure exhibits a high fidelity to the real counterpart, reproducing the fibers, ray cells and vessels. The fibers are distorted by the other fibers nearby. We can also see that the fibers are bent along the longitudinal direction due to the insertion of the ray cells along the radial direction. The vessels can emerge either isolated or grouped together in clusters.

However, this model suffers from relatively low efficiency, which is a challenge for large dataset generation for deep learning model training. This computational inefficiency is caused mainly by the microstructure distortion using the distortion map, which is the most time-consuming step in the model. For large sizes of the wood structure, generation of even a single sample may take up to several hours.

To enable large wood microstructure dataset generation, in this work we aim to accelerate the microstructure generation by developing a deep learning surrogate model. Since local distortion proved to be the most time-consuming step in the original model, the surrogate model will focus specifically on this part. In order to train the model, one needs a large dataset consisting of a variety of wood microstructures, generated by sweeping over wide ranges of structural parameters. For that purpose, we are going to develop a dataset generator, which will be described in the next subsection. Once the surrogate model has been properly trained, it can be used to replace the local distortion part in the original method.

2.2. Dataset generator

For generating a variety of wood microstructures using the method described in the paper [30], a dataset generator was developed. This generator executes the wood microstructure model up to the local distortion stage, employing a set of variable parameters to produce diverse data samples of the local distortion. It saves the pairs of generated undistorted and distorted slices in the TIFF format, along with their corresponding distortion maps in the CSV format, thereby creating a comprehensive dataset suitable for deep learning-based surrogate model development of the local distortion.

The dataset generator was implemented using the Python programming language, chosen for its availability. This generator utilizes a wood microstructure model originally implemented in MATLAB. To integrate the MATLAB code within the Python environment, the MATLAB code was modified into a callable function that accepts various parameters for wood microstructure generation. In addition, the stages after the local distortion were removed from the wood microstructure model to enhance the data generation speed specific to local distortion scenarios. The MATLAB function and its auxiliary functions were then converted into a Python package using the MATLAB compiler SDK [64].

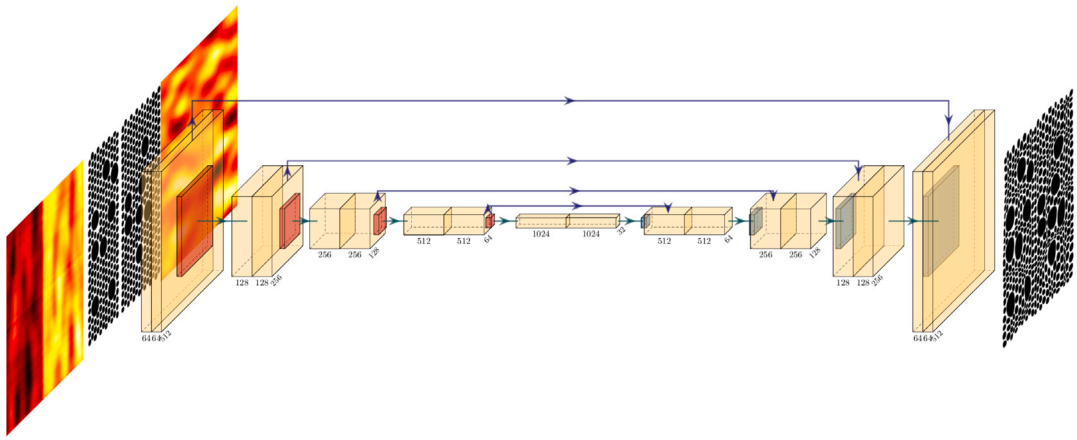

Fig. 3. Scheme of the U-Net neural network trained to perform distortion of wood microstructures. An undistorted slice of the wood microstructure and two distortion maps are fed as the input to the U-Net. As the output, a slice distorted according to the distortion map is produced.

To execute this Python package within the Python-based dataset generator, MATLAB Runtime is employed, which allows the use of compiled MATLAB applications without the need to install MATLAB [65].

The dataset generator accepts various parameter combinations as input to produce local distortion samples for different wood microstructure scenarios. For each microstructure only one slice is randomly selected. That guarantees that the whole dataset does not include slices that share too much similarity, which is important when the surrogate model is evaluated on the test set. Table 1 provides the parameters that can be adjusted for data generation along with the value ranges used for creating the dataset and their descriptions. Except when noted, the values of the parameters are chosen randomly from the uniform distribution. The unit for the length parameters are pixels. Although the dataset generator does not include all parameters from the original wood microstructure model, the wide range of adjustable parameters allows us to produce diverse locally distorted samples.

3. Training of neural networks

In this section, the architecture of the U-Net, which is employed as the surrogate model in this work, is presented. The procedure of training the U-Net is also described in detail. Transfer learning, which is a technique applied in order to improve the prediction accuracy, is also discussed here.

3.1. U-net neural network

The ML-based surrogate model for the distortion of wood microstructures is implemented within the PyTorch library of Python as a U-Net neural network, shown schematically in Fig. 3. U-Net is a type of CNN that was originally developed for biomedical image segmentation [41]. Compared to a traditional CNN, which converts an input array into a vector, the U-Net converts an array into another array of the same shape as the input, therefore making its architecture well-suited for performing image processing, such as distortion targeted in this work.

The U-Net architecture consists of the contracting path and the expanding path. Both paths are built of convolutional blocks, numbered 1 to 9 starting from the input. All the layers included in the U-Net are listed in Table 2. The input consists of three concatenated arrays representing the input image, the u- and the w-components of the distortion map as defined in Eq. (2). The input image is given as a two-dimensional array of pixels with the values representing the pixel intensity in grayscale ranging between 0 (black) and 1 (white). The distortion maps are produced by the dataset generator and are also given in form of two-dimensional arrays. No scaling or normalization is applied to the input data, and no clipping occurs. Each block of the U-Net consists of two Conv2d convolutional layers (denoted by a and b) of kernel size (3, 3). ReLU is used as the activation function in all the convolutional layers, except the last one, where the sigmoid function is used instead, so the output values of the network are in the range between 0 and 1, which corresponds to the intensity of the pixels in the images. The convolutional blocks in the contracting path end with a MaxPool2d pooling layer, which reduces the spatial size of the array by a factor of 2 in both directions, while the number of channels is doubled, starting from 64 in the first block. On the other hand, the blocks in the expanding path start with an upsampling ConvTranspose2d layer, which again doubles the spatial size in both directions, while the number of channels is reduced by a factor of 2. The 5th block, which connects the expanding and contracting path, is the bottleneck of the U-Net, having the smallest spatial size and the largest number of channels.

In addition to the forward connections between consecutive convolutional blocks, the U-Net also features skip connections between each block in the contracting path and the corresponding equally-sized block in the expanding path. The output of the ConvTranspose2d layer is concatenated with the output of the convolutional layer received through the skip connection.

3.2. Transfer learning

In order to improve the prediction accuracy of the U-Net, it is first pre-trained with images that are generated randomly and distorted according to the prescribed distortion map, analogously to wood microstructures. Afterwards, the parameters of the pre-trained U-Net are stored in a file and later used as the initial parameters for training the network with the wood microstructures. This technique, known as transfer learning, is often utilized when the data representing the target problem are scarce, however, a related problem, called in this context the source problem, for which more data are available, can be found. In the context of the image distortion studied in this work, it is important to note that the images representing slices of wood microstructures tend to be similar to each other, even when they come from separate three-dimensional structures, with the hexagonal distribution of fibers occurring in all of them. Not having enough variability in the dataset may lead to overfitting. Therefore, transfer learning can be a useful technique to improve the accuracy of the U-Net trained to perform distortion of wood microstructures.

First, in order to prepare the dataset for transfer learning, 2500 random images of size 512 × 512 pixels are generated and each of them is distorted using distortion maps in a similar way as described in Section 2. An example of such an image before and after distortion

Table 1
Parameters for the data generator with the corresponding value ranges and their descriptions.

Parameter	Value range	Description
sizeVolume (x-component)	200–500 (interval of 100)	Volume size of the microstructure.
sizeVolume (y-component)	200–500 (interval of 100)	
sizeVolume (z-component)	300 (constant)	
extraSZ (x-component)	150 (constant)	Extra volume for image interpolation.
extraSZ (y-component)	200 (constant)	
extraSZ (z-component)	100 (constant)	
Random seed	1–2000 (changed iteratively for each sample)	Random seed used to generate microstructure.
saveSlice	1–300	Number of the slice saved from generated microstructure corresponding to its longitudinal coordinate.
cellR	10–20	Average radius of fibers.
cellLength	2100–2500	Average length of fibers.
cellLengthVariance	530–630	Length variance of the fibers.
rayCellLength	50–70	Length of ray cell in radial direction.
rayCell_variance	13–17	Length deviation of ray cells in radial direction.
rayCellNum	9–13	Number of ray cells in a group of ray cells.
rayCellNumStd	2–14	Standard deviation of the number of ray cells.
vesselLength	700–900	Average length of vessels.
vesselLengthVariance	180–220	Variance of the length of vessels.
raywHeight	38–46	Height of the ray cells in direction of fiber.
raySpace	18–22	The space between ray cell groups.
isExistVessel	0 or 1	True or false representing if vessels are included.
isExistRayCell	0 or 1	True or false representing if ray cells are included.
cellWallThick	4 (constant)	Thickness of the cell wall.

is shown in Fig. 4 along with the distortion maps. Those images were chosen, rather than commonly used in transfer learning image datasets like natural images, due to their similarity to wood slice images. They are grayscale images characterized by the presence of dark speckles on the white background, similarly to the presence of different components in the wood microstructures, however, with much larger variety of shapes. The U-Net is trained with the undistorted images and the distortion maps provided as the input, and the distorted images as the output. The whole dataset is split into training, validation and test sets in the ratio 80:10:10%, respectively. The mean squared error is used as the loss function, and the network is trained with Adam optimizer with the learning rate set to $2 \cdot 10^{-4}$. The batch size is equal to 2 and the maximal number of training epochs is 1000. The model was found to be robust with respect to those hyperparameters. The early stopping is implemented with a patience of 20 epochs, after which the training is stopped if the value of the loss function evaluated on the validation set does not further decrease. The parameters of the U-Net in the epoch with the lowest loss of the validation set are stored.

The U-Net is subsequently re-trained with wood microstructures. Again, Adam optimizer is used, this time with the learning rate set to 10^{-4} and the batch size of 4. The maximal number of epochs is again 1000 and the patience for early stopping is set to 20. The dataset generator described in Section 2.2 is used to prepare a set of 2000 slices of birch microstructures with structural parameters chosen randomly within specified ranges listed in Table 1. The U-Net is fine-tuned with that dataset using the parameters obtained during the pre-training as the initial ones.

During the fine-tuning of the network, it is common to freeze some of its layers, which means that their parameters are not updated during training. For instance, in classification problems [66–68] it is very often recommended to freeze all the layers of the CNN except the output one [69]. In that kind of problem the shallow layers are responsible for detecting low-level features such as edges of the objects, while the deeper layers are responsible for detecting more high-level domain-specific features [70,71].

However, for problems other than classification tasks, the same freezing strategy might not work. Due to the different architecture of U-Net, particularly the presence of skip connections, the notion of shallow and deep layers is not as straightforward as in the ordinary CNN. In the paper [72], transfer learning was applied to ultrasound image segmentation by U-Net. Several freezing schemes of the convolutional blocks were tested and the best strategies turned out to be either fine-tuning the whole U-Net (without freezing) or only freezing Block 5, the bottleneck of the U-Net.

In this work, we perform transfer learning on the U-Net with the same freezing strategies as those studied in the paper [72]. The U-Net is fine-tuned with the set of wood microstructures starting from

Table 2
List of all the layers in the U-Net. H and W denote the height and the width of the input images, respectively.

Layer	Input shape	Activation function
conv1a	$H \times W \times 3$	ReLU
conv1b	$H \times W \times 64$	ReLU
pool1	$H \times W \times 64$	
conv2a	$\lfloor H/2 \rfloor \times \lfloor W/2 \rfloor \times 64$	ReLU
conv2b	$\lfloor H/2 \rfloor \times \lfloor W/2 \rfloor \times 128$	ReLU
pool2	$\lfloor H/2 \rfloor \times \lfloor W/2 \rfloor \times 128$	
conv3a	$\lfloor H/4 \rfloor \times \lfloor W/4 \rfloor \times 128$	ReLU
conv3b	$\lfloor H/4 \rfloor \times \lfloor W/4 \rfloor \times 256$	ReLU
pool3	$\lfloor H/4 \rfloor \times \lfloor W/4 \rfloor \times 256$	
conv4a	$\lfloor H/8 \rfloor \times \lfloor W/8 \rfloor \times 256$	ReLU
conv4b	$\lfloor H/8 \rfloor \times \lfloor W/8 \rfloor \times 512$	ReLU
pool4	$\lfloor H/8 \rfloor \times \lfloor W/8 \rfloor \times 512$	
conv5a	$\lfloor H/16 \rfloor \times \lfloor W/16 \rfloor \times 512$	ReLU
conv5b	$\lfloor H/16 \rfloor \times \lfloor W/16 \rfloor \times 1024$	ReLU
up6	$\lfloor H/16 \rfloor \times \lfloor W/16 \rfloor \times 1024$	
conv6a	$\lfloor H/8 \rfloor \times \lfloor W/8 \rfloor \times 1024$	ReLU
conv6b	$\lfloor H/8 \rfloor \times \lfloor W/8 \rfloor \times 512$	ReLU
up7	$\lfloor H/8 \rfloor \times \lfloor W/8 \rfloor \times 512$	
conv7a	$\lfloor H/4 \rfloor \times \lfloor W/4 \rfloor \times 512$	ReLU
conv7b	$\lfloor H/4 \rfloor \times \lfloor W/4 \rfloor \times 256$	ReLU
up8	$\lfloor H/4 \rfloor \times \lfloor W/4 \rfloor \times 256$	
conv8a	$\lfloor H/2 \rfloor \times \lfloor W/2 \rfloor \times 256$	ReLU
conv8b	$\lfloor H/2 \rfloor \times \lfloor W/2 \rfloor \times 128$	ReLU
up9	$\lfloor H/2 \rfloor \times \lfloor W/2 \rfloor \times 128$	
conv9a	$H \times W \times 128$	ReLU
conv9b	$H \times W \times 64$	sigmoid

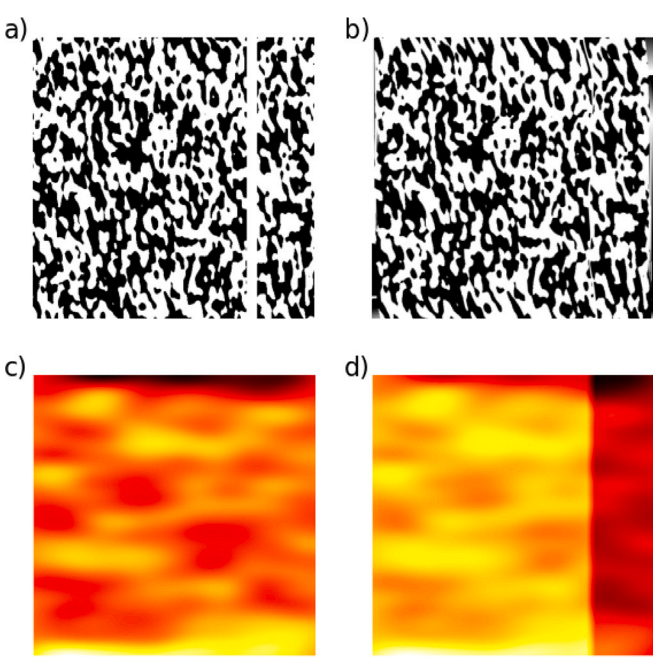

Fig. 4. A single random image used for pre-training the U-Net: (a) before distortion, (b) after distortion, (c) u-element of the distortion map, (d) w-element of the distortion map.

Table 3
Frozen layers during training the neural network with wood microstructures.

Neural network	Frozen blocks
0	from scratch
1	5b–9
2	1–5a
3	2–9
4	1–8
5	3–9
6	1–2,5–9
7	5
8	1–4,6–9
9	3–7
10	1–2,8–9
11	2–8
12	no frozen blocks

the parameters obtained from pre-training with random structures. Moreover, we also train another network from scratch, which means that its parameters are initialized randomly rather than transferred from the pre-trained network. All the strategies applied are summarized in Table 3. We evaluate the score for the test set for each of the strategies applied and compare them with each other.

4. Results

The full dataset of wood microstructures consists of 2000 slices. In order to assess how the performance of the U-Net depends on the training set size, the model is trained both on the entire set and its subsets. Training it on a smaller subset also makes sense in the context of transfer learning, which is particularly useful for improving the performance of the neural network when the set of available data is scarce.

Additionally, during training, k-fold cross-validation is applied. The dataset (either entire or its chosen subset) is divided into $k = 5$ separate equal-sized folds, and the U-Net is trained k times, each time with different portions of the whole dataset used as training, validation and test set. In each iteration one fold is used as the test set while the configurations in the remaining $k - 1$ folds are split into training and validation sets in the ratio $90 : 10\%$.

The training of the U-Net is performed on AMD MI250x GPU of the LUMI supercomputer. The total training trained on all 5 folds ranged between 2 and 43 h, depending on the freezing scheme, which influenced how fast the training converged.

4.1. Model validation

The surrogate model is validated for interpolation within the sampled parameter space. In Fig. 5, the root mean square error (RMSE) determined for the test set is shown for the U-Net trained on the subset of 100 slices both from scratch and using transfer learning with all the freezing strategies considered. It can be seen that some of those transfer learning strategies (represented by the green bars) outperform the training from scratch. In all of those strategies, the bottleneck of the U-Net, Block 5, is frozen (either entirely or only its second half denoted by 5b). In contrast, freezing all blocks except the bottleneck produces by far the worst results of all the strategies tested. Moreover, the common transfer learning strategy used in image classification by CNN, where all the blocks are frozen except for the last one (here 1-8), also produces much worse results than training from scratch. These results suggest that Block 5 is responsible for task-specific processing in the U-Net, while the blocks closer to the input and output are more responsible for domain-specific processing.

In Fig. 6 the mean absolute error (MAE) for the test set for the same neural networks is shown. Compared to RMSE it can be seen that according to MAE there are more freezing schemes for which the U-Net

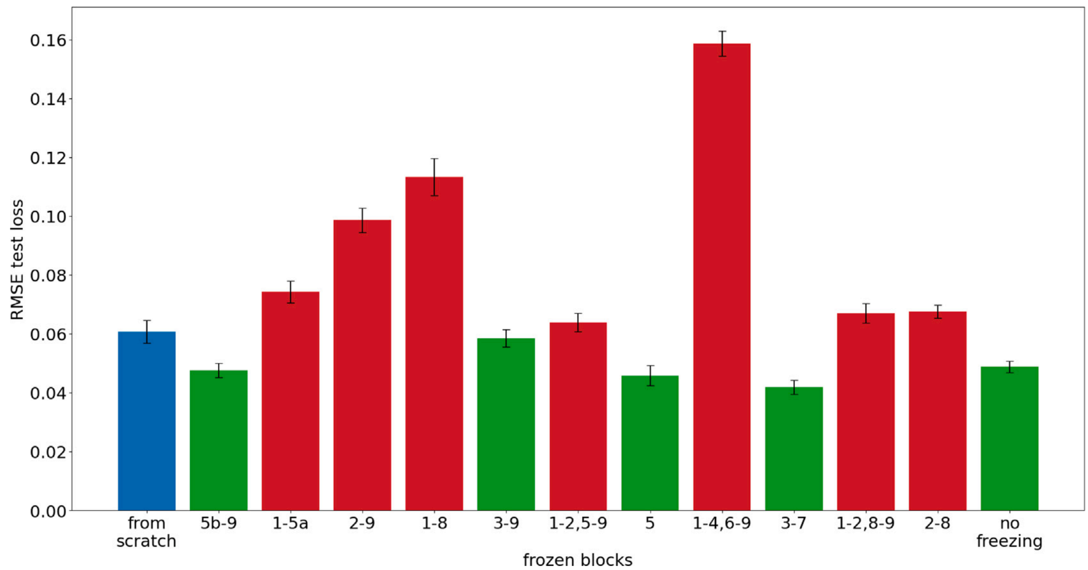

Fig. 5. Root mean square error (RMSE) determined for the test set with the U-Net trained on the subset of 100 wood slices for different freezing schemes in transfer learning compared to training from scratch. The green bars indicate the loss lower than that for the network trained from scratch (shown as the blue bar), while the red bars indicate a higher loss.

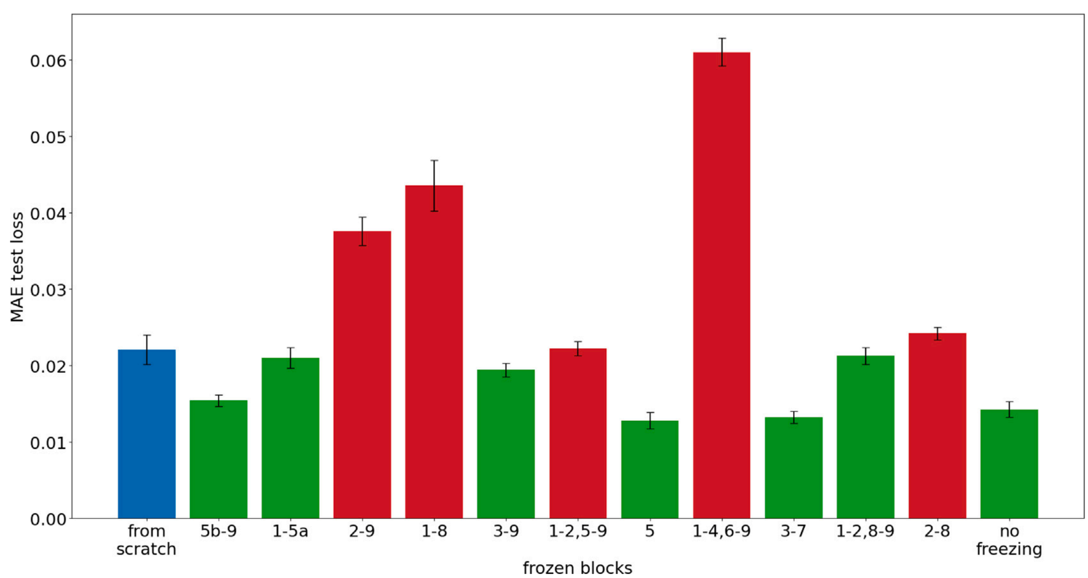

Fig. 6. Mean absolute error (MAE) determined for the test set with the U-Net trained on the subset of 100 wood slices for different freezing schemes in transfer learning compared to training from scratch. The green bars indicate the loss lower than that for the network trained from scratch (shown as the blue bar), while the red bars indicate a higher loss.

outperforms the network trained from scratch. It can be related to the fact that RMSE is more sensitive to outliers compared to MAE due to the square function.

Finally, in Fig. 7 the structural similarity index measure (SSIM) for the test set obtained for different neural networks is shown. SSIM is a common quantity for measuring the similarity between two images. Its value is in the range between −1 and 1, where 1 indicates perfect similarity, 0 no similarity and −1 perfect anti-correlation. It can be seen in Fig. 7 that SSIM is close to 1 for many neural networks, with some of the fine-tuned networks outperforming the one trained from scratch.

In Fig. 8 the local distortion performed by the U-Net trained with and without transfer learning is compared on a single wood slice containing fibers, vessels and ray cells. The same slice distorted by the original distortion-map-based model is shown there as a reference. It can be seen there that the structure predicted by the U-Net trained with transfer learning is slightly more accurate than the one obtained by the U-Net trained from scratch. In particular, distortion of the ray cells is more accurately reproduced when using transfer learning.

In Fig. 9 RMSE for the test set is shown for the U-Net trained with the entire dataset of 2000 wood slices, again comparing different transfer learning strategies and training from scratch. It can be seen that according to RMSE employing transfer learning does not further improve the training in the case of the full set being used. However, as shown in Fig. 10, MAE is slightly lower for two strategies employing transfer learning than for training from scratch. In Fig. 11 SSIM is shown for the full test. The same strategies for which MAE was smaller than that of the network trained scratch, result also in the higher SSIM value, indicating higher similarity.

In Fig. 12 a 3D birch microstructure of size 550 × 500 × 300 generated by the original method is compared with that generated by the surrogate model trained without and with transfer learning (with Block 5 frozen). It can be observed that the final structure

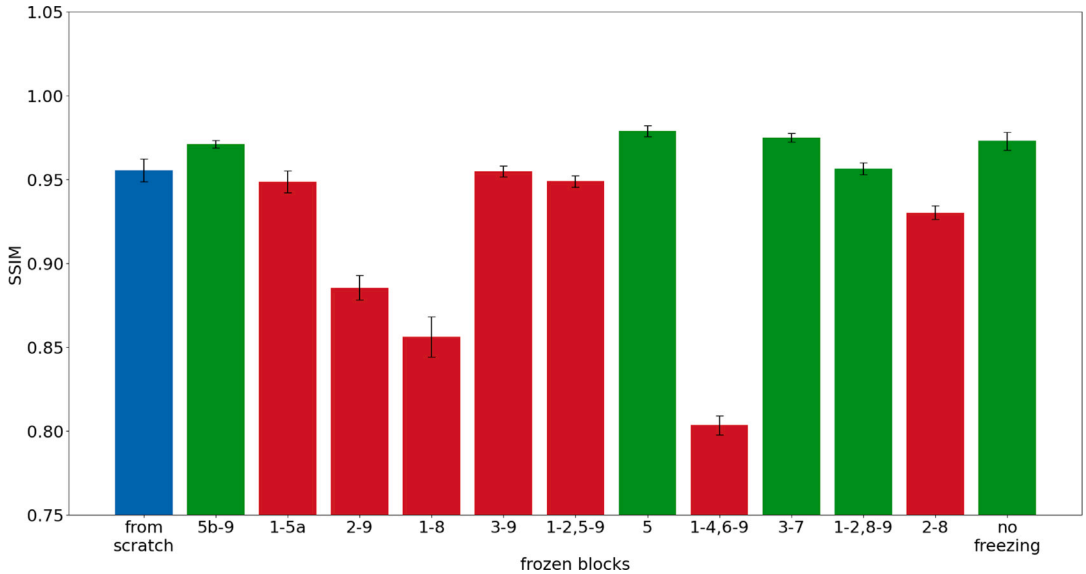

Fig. 7. Structural similarity index measure (SSIM) determined for the test set with the U-Net trained on the subset of 100 wood slices for different freezing schemes in transfer learning compared to training from scratch. The green bars indicate the SSIM higher than that for the network trained from scratch (shown as the blue bar), while the red bars indicate a lower SSIM.

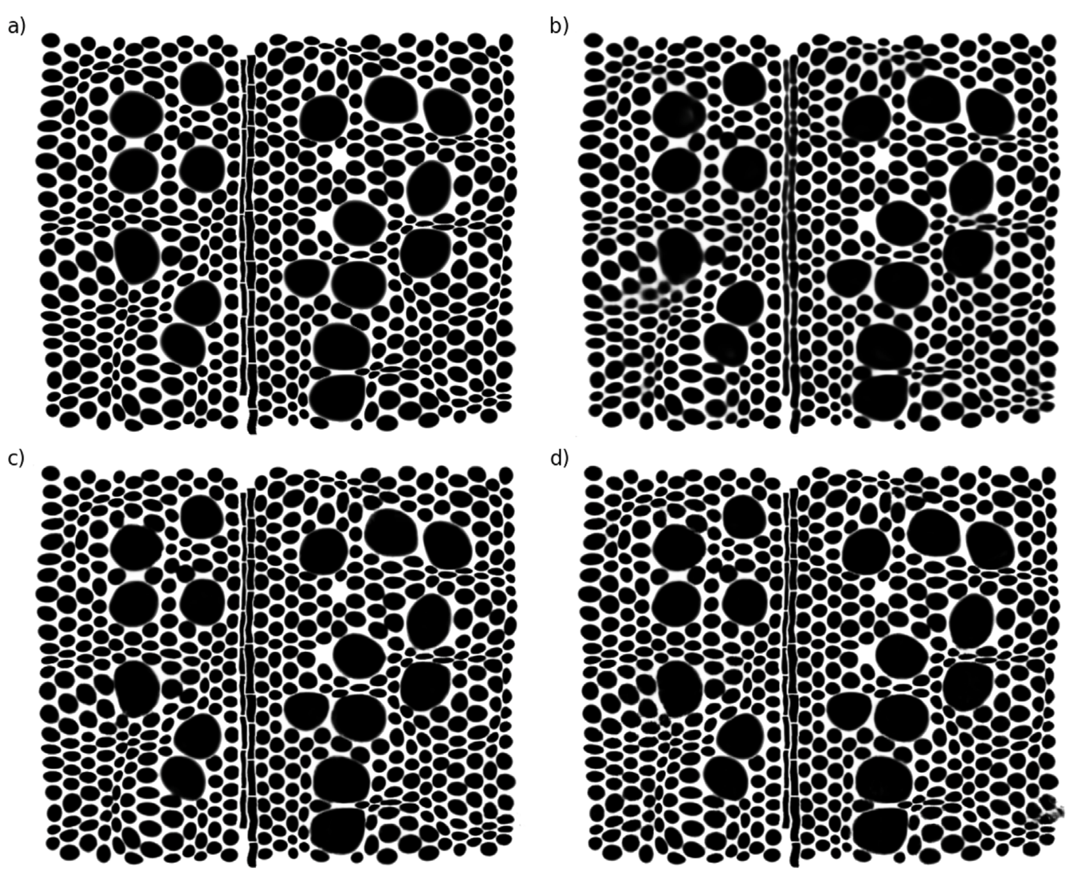

Fig. 8. A locally distorted slice of a wood microstructure obtained with different methods: (a) generated by the original method with a prescribed distortion map, (b) predicted by the U-Net trained from scratch, (c) using transfer learning with Block 5 frozen, (d) with Blocks 3-7 frozen.

generated by the surrogate model is accurately reproduced. However, in order to assess the accuracy quantitatively, the Euler characteristic is determined for all three microstructures, defined as the number of objects plus the number of holes, minus the number of tunnels or loops. Its value for the sample created by the original method is 603, while for the sample created with the surrogate model trained from scratch and with transfer learning is 506 and 586, respectively. While for this specific microstructure the Euler characteristic value was reproduced more accurately for the surrogate model trained with transfer learning, this did not hold for the other microstructures that were tested. For some of them the Euler characteristic was more accurately reproduced without transfer learning.

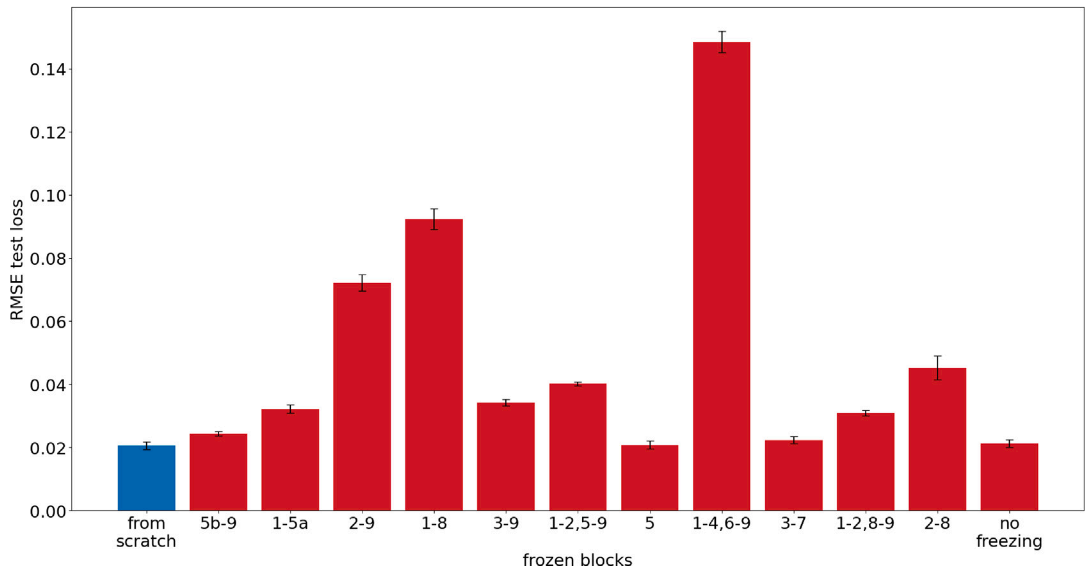

Fig. 9. Root mean square error (RMSE) determined for the test set with the U-Net trained on the full set of 2000 wood slices for different freezing schemes in transfer learning compared to training from scratch. In this case the loss obtained with transfer learning (red bars) is always higher than that for the network trained from scratch (shown as the blue bar).

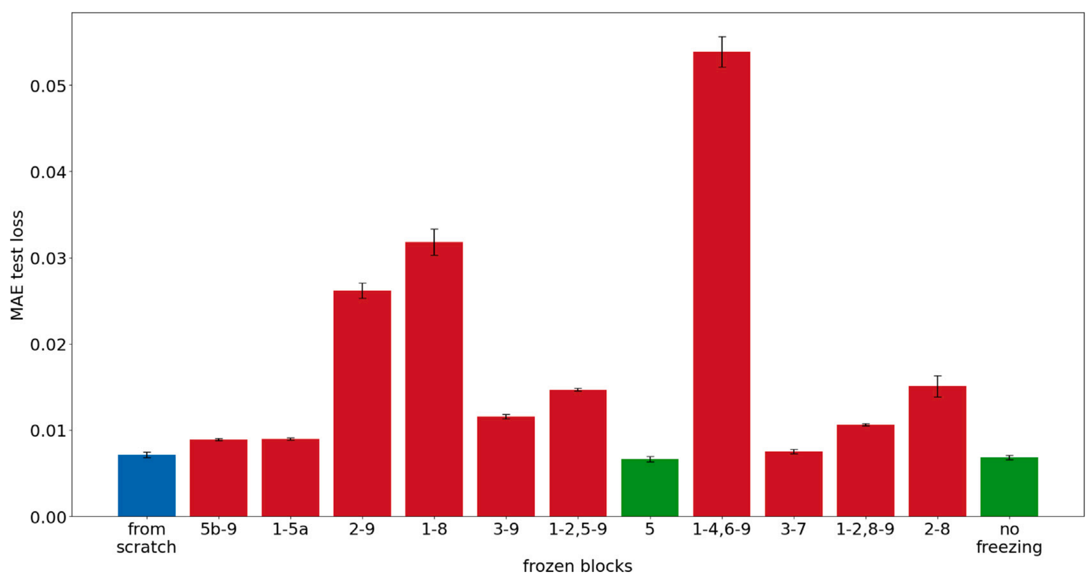

Fig. 10. Mean average error (MAE) determined for the test set with the U-Net trained on the full set of 2000 wood slices for different freezing schemes in transfer learning compared to training from scratch. The green bars indicate the loss lower than that for the network trained from scratch (shown as the blue bar), while the red bars indicate a higher loss.

4.2. Speed-up

The runtime for all the steps of generating the birch microstructure of the size 550 × 500 × 300 has been compared between different methods and summarized in Table 4. It shows the timing breakdown for the pipeline employing the original method on CPU, the GPU-accelerated interpolation and the surrogate model on GPU. It can be seen that the time for the local distortion is greatly reduced while using the surrogate model, which also contributes to a significant reduction of the total generation time.

As the interpolator LinearNDInterpolator from the CuPy library was chosen, which provides the exact numerical baseline. On the other hand, the surrogate model offers a speed-up, which is advantageous when small approximation errors are acceptable. Both the surrogate model and the GPU-accelerated interpolation were run on NVIDIA V100 GPU on the Aalto University's Triton cluster.

4.3. Optical scattering

Since the motivation for developing the surrogate model is speeding-up the generation of wood microstructures, which in turn can be useful for faster parametric study, in this section we provide a comparison of the optical properties obtained for the same sample generated both with and without the surrogate model.

A wood microstructure of the size 750 × 500 × 750 was created. The optical scattering was studied using the ray tracing method [31,73]. The ray propagates along the y-direction. The refractive index for the fibers is set to 1.54 and for the matrix 1.52. The obtained haze parameters are 7.7309% (x-direction) and 62.8514% (z-direction) for the sample generated without the surrogate, and 7.4148% (x-direction) and 65.0301% (z-direction) for the same sample generated with the surrogate model trained from scratch, and 7.7387% (x-direction) and 64.7236% (z-direction) with the surrogate model trained using transfer

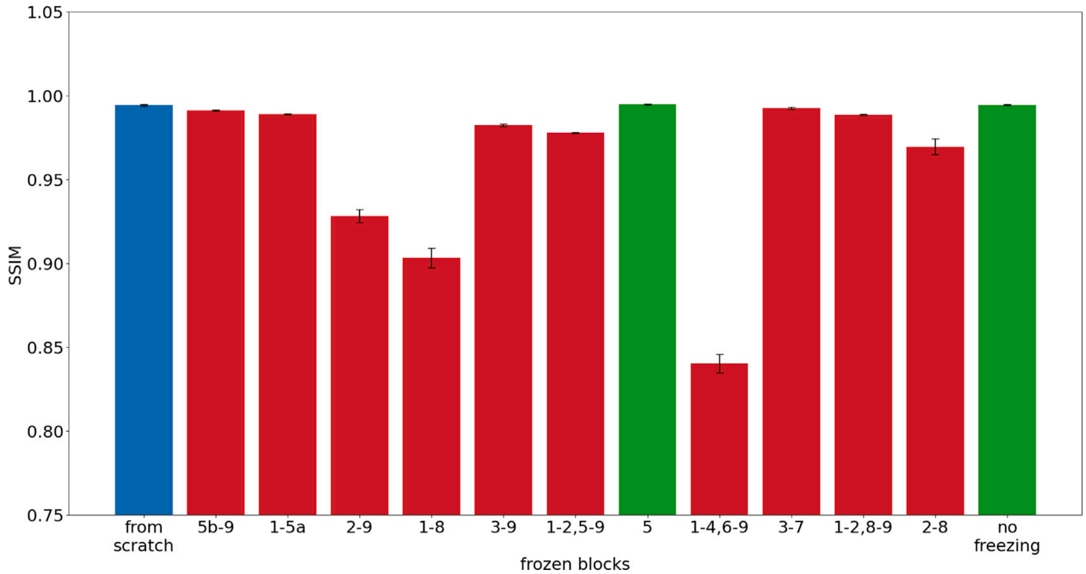

Fig. 11. Structural similarity index measure (SSIM) determined for the test set with the U-Net trained on the full set of 2000 wood slices for different freezing schemes in transfer learning compared to training from scratch. The green bars indicate the SSIM higher than that for the network trained from scratch (shown as the blue bar), while the red bars indicate a lower SSIM.

Table 4
Timing breakdown of generation of a birch microstructure of the size $550 \times 500 \times 300$ with the surrogate model, with the GPU-accelerated interpolation and with the original method.

Step	Surrogate [s]	CuPy [s]	Original method [s]
I/O	236.7 ± 0.7	330 ± 10	313 ± 4
Ray cells	32.3 ± 0.4	32 ± 3	35 ± 2
Vessels	0.00232 ± 0.00007	0.2 ± 0.4	0.04 ± 0.03
Small fibers	30.3 ± 0.8	31 ± 3	31 ± 1
Large fibers	4.35 ± 0.03	5.0 ± 0.1	5.3 ± 0.4
Distortion maps	6.62 ± 0.08	7.5 ± 0.4	8.7 ± 0.1
Ray cell shrinking	20.9 ± 0.4	23 ± 2	23.6 ± 0.6
Local distortion	28.0 ± 0.2	52 ± 3	2350 ± 20
Global distortion	80.5 ± 0.3	85 ± 2	123 ± 2
Total	440 ± 1	570 ± 20	2880 ± 20

learning with Block 5 frozen. This test suggests that for this specific sample the surrogate model is able to preserve the relevant optical response.

5. Conclusions

In this work, an ML-based surrogate model for performing local distortion within wood microstructure generation has been developed. The U-Net architecture was chosen for the model because of its ability to perform an image-to-image transformation, which can model the local distortion, the most time-consuming step in the generation of wood microstructures. Unlike the original U-Net, which is commonly applied to image segmentation, the model used in this work requires, in addition to the original undistorted image, two additional arrays representing distortion maps to be given as the input.

After being trained with a sufficiently large dataset, the U-Net performs local distortion with accuracy comparable to the original distortion-map-based model developed in the paper [30], which had been shown to produce wood microstructures exhibiting excellent agreement with SEM images. This result suggests that the model is able to generate wood microstructures compatible with those generated by the physics-based model. The surrogate model can be applied to a slice of a wood microstructure of arbitrary size, containing fibers, vessels, and ray cells. Of all those elements of the structure, the distortion of ray cells turned out to be the most challenging for the surrogate model. It was observed that for the U-Net trained with a small number of samples, the distorted ray cells were not represented as accurately as fibers and vessels. However, after increasing the size of the dataset, the accuracy improved significantly.

Under the tested pre-training and fine-tuning setup, transfer learning was found to be useful for improving the predictions of the U-Net compared to training the network from scratch. That gain could be a result of the pre-training distribution, smoother initialization or a regularization effect. The improvement was particularly noticeable when for training and fine-tuning the U-Net, a limited dataset of wood microstructures was used instead of the full available set. In particular, distortion of the ray cells was more accurately reproduced with a fine-tuned neural network than the network trained from scratch, even without expanding the dataset.

Several strategies for freezing the convolutional blocks of the U-Net during transfer learning were tested and compared. Contrary to the classification problems carried out by a traditional CNN, for which freezing the early layers is often the most optimal strategy, in the problem of image distortion studied in this work fine-tuning the whole network or freezing only its bottleneck turned out to be the best approaches. This is in agreement with the results obtained earlier for fine-tuning the U-Net for the segmentation of medical images [72]. This result suggests that in tasks involving image-to-image transformation, the bottleneck contains information specific to the process of transformation, independent of the actual input, therefore, it does not need to be fine-tuned when the network is re-trained for a different type of input. On the other hand, convolutional blocks outside the bottleneck are responsible for processing the data related to the specific input.

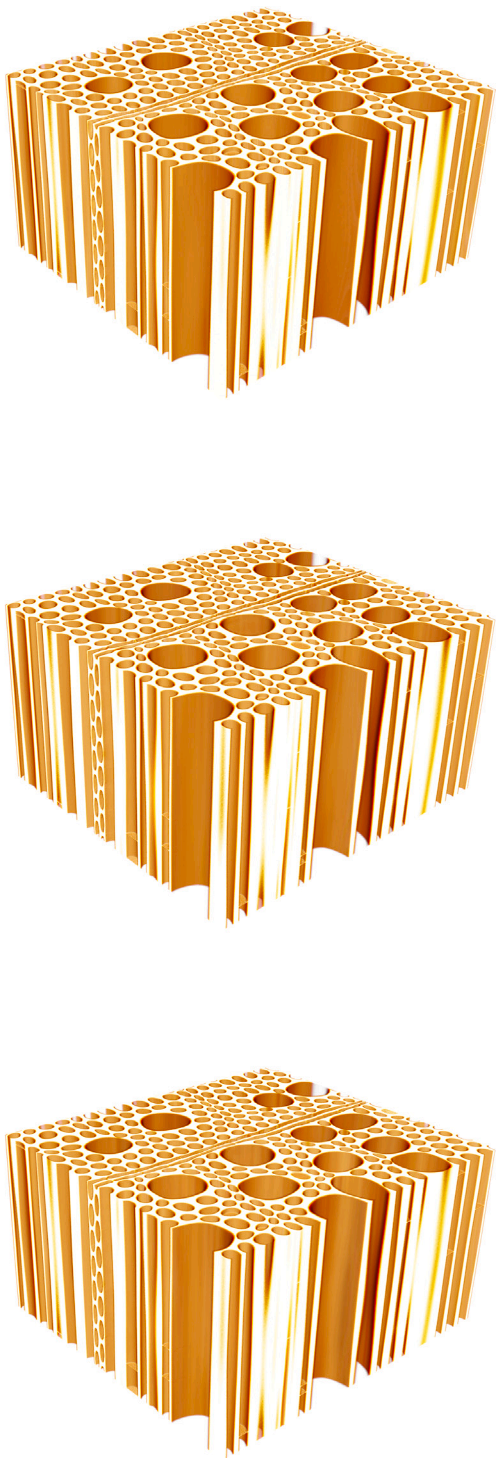

Fig. 12. A 3D birch microstructure of the size 550 × 500 × 300 generated by the original method (top), the surrogate model without transfer learning (middle) and the surrogate model with transfer learning (bottom).

Because the surrogate model has been trained for a specific type of wood, namely birch, it is not expected to work for other materials or outside the range of the parameters it was trained on without re-training it on a new dataset. However, as shown in this work, using transfer learning may help to reduce the computational resources needed to retrain the model compared to training it from scratch.

While the U-Net-based surrogate model developed in this work provides a significant speed-up of the wood microstructure generation with good accuracy, comparing it with other surrogate models, such as generative adversarial network (GAN) or diffusion models, would be an interesting subject for further research. However, the advantage of the U-Net is that it can be trained with a relatively small dataset. Moreover, while the current surrogate model uses the backbone structure created by the physical model as the input, it does not contain any physical constraints relevant for the distortion, which may result in inaccuracies in the final structure. Implementing physics-related constraints for the final structure would be an interesting step in developing the model further.

The surrogate model is a promising tool for generating a large dataset of wood microstructures in a relatively short time compared to the original method. The backbone structure can still be generated by the original code while the distortion procedure can be replaced by the surrogate model. Generating a varied dataset of wood samples in a short time can be beneficial for the parameter study, where the goal is to optimize some physical properties with respect to the structural parameters. In the context of transparent wood, the surrogate model can be helpful to achieve the optimal optical transmittance and mechanical strength. It has been shown that the surrogate model preserves the haze parameters of the single tested sample, however, further work is required for broader property validation.

CRediT authorship contribution statement

Marcin Mińkowski: Writing – review & editing, Writing – original draft, Visualization, Validation, Software, Methodology, Investigation, Data curation, Conceptualization. **Fahime Seyedheydari:** Writing – review & editing. **Mikko Seppi:** Writing – review & editing, Software, Methodology. **Bin Chen:** Writing – review & editing, Software, Methodology, Conceptualization. **Davide Grassano:** Writing – review & editing, Software. **Simo Särkkä:** Writing – review & editing, Supervision, Resources, Project administration, Funding acquisition, Conceptualization.

Declaration of competing interest

The authors declare that they have no known competing financial interests or personal relationships that could have appeared to influence the work reported in this paper.

Acknowledgments

The authors thank the HORIZON AI-TRANSPWOOD (AI-Driven Multiscale Methodology to Develop Transparent Wood as Sustainable Functional Material) project, Grant no. 101138191, co-funded by the European Union. Views and opinions expressed are however those of the author(s) only and do not necessarily reflect those of the European Union or HaDEA. Neither the European Union nor the granting authority can be held responsible for them. We acknowledge CSC (Finland) for awarding this project access to the LUMI supercomputer, owned by the EuroHPC Joint Undertaking, hosted by CSC (Finland) and the LUMI consortium through CSC (Finland).

Data availability

The data presented in this study are available from the corresponding author upon request. The code for the original MATLAB implementation of the physics-based model for wood microstructure generation, the dataset generator and the Python training script for the surrogate model are available on GitHub (https://github.com/MarcinMinkowski/wood-microstructure-surrogate/tree/main/wood-microstructure. The code for the Python implementation of the wood microstructure generation model employing the surrogate is available at https://github.com/AI-TranspWood/AITW_microstructures.

References

[1] W.B. Chaabene, M. Flah, M.L. Nehdi, Machine learning prediction of mechanical properties of concrete: Critical review, Constr. Build. Mater. 260 (2020) 119889.

[2] H.S. Stein, D. Guevarra, P.F. Newhouse, E. Soedarmadji, J.M. Gregoire, Machine learning of optical properties of materials–predicting spectra from images and images from spectra, Chem. Sci. 10 (2019) 47–55.

[3] X. Qian, R. Yang, Machine learning for predicting thermal transport properties of solids, Mater. Sci. Eng.: R: Rep. 146 (2021) 100642.

[4] J. Li, Q. Zhang, R. Huang, X. Li, H. Gao, Towards understanding the structure–property relationships of heterogeneous-structured materials, Scr. Mater. 186 (2020) 304–311.

[5] S.M. Moosavi, K.M. Jablonka, B. Smit, The role of machine learning in the understanding and design of materials, J. Am. Chem. Soc. 142 (48) (2020) 20273–20287.

[6] A.R. Oganov, C.J. Pickard, Q. Zhu, R.J. Needs, Structure prediction drives materials discovery, Nat. Rev. Mater. 4 (5) (2019) 331–348.

[7] X. Wan, W. Feng, Y. Wang, H. Wang, X. Zhang, C. Deng, N. Yang, Materials discovery and properties prediction in thermal transport via materials informatics: a mini review, Nano Lett. 19 (6) (2019) 3387–3395.

[8] T.-S. Vu, M.-Q. Ha, D.-N. Nguyen, V.-C. Nguyen, Y. Abe, T. Tran, H. Tran, H. Kino, T. Miyake, K. Tsuda, et al., Towards understanding structure–property relations in materials with interpretable deep learning, Npj Comput. Mater. 9 (1) (2023) 215.

[9] M. Bhong, T.K. Khan, K. Devade, B.V. Krishna, S. Sura, H. Eftikhaar, H.P. Thethi, N. Gupta, Review of composite materials and applications, Mater. Today: Proc. (2023).

[10] M. Hasan, J. Zhao, Z. Jiang, Micromanufacturing of composite materials: a review, Int. J. Extrem. Manuf. 1 (1) (2019) 012004.

[11] S. Fink, Transparent wood–a new approach in the functional study of wood structure, Holzforschung (1992).

[12] Y. Li, Q. Fu, S. Yu, M. Yan, L. Berglund, Optically transparent wood from a nanoporous cellulosic template: combining functional and structural performance, Biomacromolecules 17 (4) (2016) 1358–1364.

[13] M. Zhu, J. Song, T. Li, A. Gong, Y. Wang, J. Dai, Y. Yao, W. Luo, D. Henderson, L. Hu, Highly anisotropic, highly transparent wood composites., Adv. Mater. (Deerfield Beach Fla.) 28 (26) (2016) 5181–5187.

[14] E. Jungstedt, C. Montanari, S. Östlund, L. Berglund, Mechanical properties of transparent high strength biocomposites from delignified wood veneer, Compos. Part A: Appl. Sci. Manuf. 133 (2020) 105853.

[15] Y. Li, E. Vasileva, I. Sychugov, S. Popov, L. Berglund, Optically transparent wood: recent progress, opportunities, and challenges, Adv. Opt. Mater. 6 (14) (2018) 1800059.

[16] F. Jiang, T. Li, Y. Li, Y. Zhang, A. Gong, J. Dai, E. Hitz, W. Luo, L. Hu, Wood-based nanotechnologies toward sustainability, Adv. Mater. 30 (1) (2018) 1703453.

[17] A. Mariani, G. Malucelli, Transparent wood-based materials: Current state-of-the-art and future perspectives, Materials 15 (24) (2022) 9069.

[18] J. Zhang, A. Koubaa, Y. Tao, P. Li, D. Xing, The emerging development of transparent wood: Materials, characteristics, and applications, Curr. For. Rep. 8 (4) (2022) 333–345.

[19] X. Hu, R. Yu, F. Wang, Z. Liu, H. Yang, C. Chen, Y. Li, N. Noor, B. Fei, Fabrication, functionalities and applications of transparent wood: a review, Adv. Funct. Mater. 33 (37) (2023) 2303278.

[20] H. Harada, W. Côté, Structure of wood, Biosynth. Biodegrad. Wood Compon. 1 (1985) 1–42.

[21] G. Daniel, Wood and fibre morphology, Wood Chem. Wood Biotechnol. 1 (2009) 45–70.

[22] S. Carlquist, Living cells in wood. 1. Absence, scarcity and histology of axial parenchyma as keys to function, Bot. J. Linean. Soc. 177 (3) (2015) 291–321.

[23] J. Pang, A. Baitenov, C. Montanari, A. Samanta, L. Berglund, S. Popov, I. Zozoulenko, Light propagation in transparent wood: efficient ray-tracing simulation and retrieving an effective refractive index of wood scaffold, Adv. Photonics Res. 2 (11) (2021) 2100135.

[24] A. Kienle, C. D'Andrea, F. Foschum, P. Taroni, A. Pifferi, Light propagation in dry and wet softwood, Opt. Express 16 (13) (2008) 9895–9906.

[25] M. Zhu, Y. Li, F. Chen, X. Zhu, J. Dai, Y. Li, Z. Yang, X. Yan, J. Song, Y. Wang, et al., Plasmonic wood for high-efficiency solar steam generation, Adv. Energy Mater. 8 (4) (2018) 1701028.

[26] Z.-L. Yu, N. Yang, L.-C. Zhou, Z.-Y. Ma, Y.-B. Zhu, Y.-Y. Lu, B. Qin, W.-Y. Xing, T. Ma, S.-C. Li, et al., Bioinspired polymeric woods, Sci. Adv. 4 (8) (2018) eaat7223.

[27] Y. Chai, S. Liang, Y. Zhou, L. Lin, F. Fu, 3D microscale heat transfer model of the thermal properties of wood-metal functional composites based on the microstructure, Materials 12 (17) (2019) 2709.

[28] M.B. Pecha, M. Garcia-Perez, T.D. Foust, P.N. Ciesielski, Estimation of heat transfer coefficients for biomass particles by direct numerical simulation using microstructured particle models in the laminar regime, ACS Sustain. Chem. Eng. 5 (1) (2017) 1046–1053.

[29] P.N. Ciesielski, M.F. Crowley, M.R. Nimlos, A.W. Sanders, G.M. Wiggins, D. Robichaud, B.S. Donohoe, T.D. Foust, Biomass particle models with realistic morphology and resolved microstructure for simulations of intraparticle transport phenomena, Energy Fuels 29 (1) (2015) 242–254.

[30] B. Chen, C. Montanari, S. Popov, L.A. Berglund, A distortion-map-based method for morphology generation in multi-phase materials-application to wood, Compos. Sci. Technol. 244 (2023) 110262.

[31] B. Chen, S. Popov, L.A. Berglund, Ray scattering in fiber-reinforced transparent wood composites–wood microstructural effects and virtual camera simulation, Opt. Mater. 162 (2025) 116953.

[32] F. Kibrete, T. Trzepieciński, H.S. Gebremedhen, D.E. Woldemichael, Artificial intelligence in predicting mechanical properties of composite materials, J. Compos. Sci. 7 (9) (2023) 364.

[33] G. Pilania, C. Wang, X. Jiang, S. Rajasekaran, R. Ramprasad, Accelerating materials property predictions using machine learning, Sci. Rep. 3 (1) (2013) 2810.

[34] S. Chibani, F.-X. Coudert, Machine learning approaches for the prediction of materials properties, Apl Mater. 8 (8) (2020).

[35] D.W. Abueidda, M. Almasri, R. Ammourah, U. Ravaioli, I.M. Jasiuk, N.A. Sobh, Prediction and optimization of mechanical properties of composites using convolutional neural networks, Compos. Struct. 227 (2019) 111264.

[36] C. Yang, Y. Kim, S. Ryu, G.X. Gu, Using convolutional neural networks to predict composite properties beyond the elastic limit, MRS Commun. 9 (2) (2019) 609–617.

[37] X. Liu, Z. Li, S. Song, H. Li, H. Suo, W. Liu, D. Liu, Y. Song, An insulating composite material defects detection CNN model using knowledge-based 2D structured ultrasonic signals, Eng. Res. Express 6 (4) (2024) 045265.

[38] A. Cecen, H. Dai, Y.C. Yabansu, S.R. Kalidindi, L. Song, Material structure-property linkages using three-dimensional convolutional neural networks, Acta Mater. 146 (2018) 76–84.

[39] C. Li, W. He, X. Nie, X. Wei, H. Guo, X. Wu, H. Xu, T. Zhang, X. Liu, Intelligent damage recognition of composite materials based on deep learning and ultrasonic testing, AIP Adv. 11 (12) (2021).

[40] A. Shukla, G. Kalnoor, A. Kumar, N. Yuvaraj, R. Manikandan, M. Ramkumar, Improved recognition rate of different material category using convolutional neural networks, Mater. Today: Proc. 81 (2023) 947–950.

[41] O. Ronneberger, P. Fischer, T. Brox, U-net: Convolutional networks for biomedical image segmentation, in: Medical Image Computing and Computer-Assisted Intervention–MICCAI 2015: 18th International Conference, Munich, Germany, October 5-9, 2015, Proceedings, Part III 18, Springer, 2015, pp. 234–241.

[42] W. Weng, X. Zhu, INet: convolutional networks for biomedical image segmentation, IEEE Access 9 (2021) 16591–16603.

[43] H. Zunair, A.B. Hamza, Sharp U-Net: Depthwise convolutional network for biomedical image segmentation, Comput. Biol. Med. 136 (2021) 104699.

[44] P. Isola, J.-Y. Zhu, T. Zhou, A.A. Efros, Image-to-image translation with conditional adversarial networks, in: Proceedings of the IEEE Conference on Computer Vision and Pattern Recognition, 2017, pp. 1125–1134.

[45] J. Mustaniemi, J. Kannala, J. Matas, S. Särkkä, J. Heikkilä, LSD_2–joint denoising and deblurring of short and long exposure images with CNNs, in: The 31st British Machine Vision Virtual Conference, British Machine Vision Association, 2020.

[46] H. Agrawal, A. Hietanen, S. Särkkä, Deep learning based projection domain metal segmentation for metal artifact reduction in cone beam computed tomography, IEEE Access 11 (2023) 100371–100382.

[47] H. Agrawal, A. Hietanen, S. Särkkä, Deep learning architecture for scatter estimation in cone-beam computed tomography head imaging with varying field-of-measurement settings, J. Med. Imaging 11 (5) (2024) 053501.

[48] H. Agrawal, A. Hietanen, S. Särkkä, Utilizing U-Net architectures with auxiliary information for scatter correction in CBCT across different field-of-view settings, in: Medical Imaging 2024: Physics of Medical Imaging, vol. 12925, SPIE, 2024, pp. 613–617.

[49] Z. Zhang, Q. Liu, Y. Wang, Road extraction by deep residual U-Net, IEEE Geosci. Remote. Sens. Lett. 15 (5) (2018) 749–753.

[50] M.J. Khan, P.P. Singh, Advanced road extraction using CNN-based U-Net model and satellite imagery, E-Prime-Adv. Electr. Eng. Electron. Energy 5 (2023) 100244.

[51] X. Wu, D. Hong, J. Chanussot, UIU-Net: U-net in U-Net for infrared small object detection, IEEE Trans. Image Process. 32 (2022) 364–376.

[52] X. Wu, D. Hong, Z. Huang, J. Chanussot, Infrared small object detection using deep interactive U-Net, IEEE Geosci. Remote. Sens. Lett. 19 (2022) 1–5.

[53] Y. Gao, J. Jia, L. Cai, M. Zhou, H. Chai, J. Jia, A method of image restoration for distortion of object in water-air cross-media, Int. J. Distrib. Sens. Networks 2024 (1) (2024) 8442383.

[54] S. Mondal, S. Paul, N. Singh, R.K. Saha, Deep learning on photoacoustic tomography to remove image distortion due to inaccurate measurement of the scanning radius, Biomed. Opt. Express 14 (11) (2023) 5817–5832.

[55] Y. Wang, F. Ye, X. Chen, J. Xi, Image restoration of underwater fuel assembly thermal turbulence based on improved U-net network, Nucl. Eng. Technol. 57 (9) (2025) 103615.

[56] L. Torrey, J. Shavlik, Transfer learning, in: Handbook of Research on Machine Learning Applications and Trends: Algorithms, Methods, and Techniques, IGI global, 2010, pp. 242–264.

[57] K. Weiss, T.M. Khoshgoftaar, D. Wang, A survey of transfer learning, J. Big Data 3 (2016) 1–40.
[58] J. Yosinski, J. Clune, Y. Bengio, H. Lipson, How transferable are features in deep neural networks? Adv. Neural Inf. Process. Syst. 27 (2014).
[59] R. Zoetmulder, E. Gavves, M. Caan, H. Marquering, Domain-and task-specific transfer learning for medical segmentation tasks, Comput. Methods Programs Biomed. 214 (2022) 106539.
[60] R. Wu, Y. Xin, J. Qian, Y. Dong, A multi-scale interactive U-net for pulmonary vessel segmentation method based on transfer learning, Biomed. Signal Process. Control. 80 (2023) 104407.
[61] A. Pourmahboubi, N. Arsalani Saeed, H. Tabrizchi, A brain tumor segmentation enhancement in MRI images using U-Net and transfer learning, BMC Med. Imaging 25 (1) (2025) 307.
[62] D. Cheng, E.Y. Lam, Transfer learning U-Net deep learning for lung ultrasound segmentation, 2021, arXiv preprint arXiv:2110.02196.
[63] L. Alzubaidi, M. Al-Amidie, A. Al-Asadi, A.J. Humaidi, O. Al-Shamma, M.A. Fadhel, J. Zhang, J. Santamaría, Y. Duan, Novel transfer learning approach for medical imaging with limited labeled data, Cancers 13 (7) (2021) 1590.
[64] The MathWorks, Inc., Generate Python Package and Build Python Application. URL https://se.mathworks.com/help/compiler_sdk/gs/create-a-python-application-with-matlab-code.html.
[65] The MathWorks, Inc., MATLAB Runtime. URL https://se.mathworks.com/products/compiler/matlab-runtime.html.
[66] H.E. Kim, A. Cosa-Linan, N. Santhanam, M. Jannesari, M.E. Maros, T. Ganslandt, Transfer learning for medical image classification: a literature review, BMC Med. Imaging 22 (1) (2022) 69.
[67] M. Shaha, M. Pawar, Transfer learning for image classification, in: 2018 Second International Conference on Electronics, Communication and Aerospace Technology, ICECA, IEEE, 2018, pp. 656–660.
[68] M. Bansal, M. Kumar, M. Sachdeva, A. Mittal, Transfer learning for image classification using VGG19: Caltech-101 image data set, J. Ambient. Intell. Humaniz. Comput. (2023) 1–12.
[69] Z. Ardalan, V. Subbian, Transfer learning approaches for neuroimaging analysis: a scoping review, Front. Artif. Intell. 5 (2022) 780405.
[70] M. Iman, H.R. Arabnia, K. Rasheed, A review of deep transfer learning and recent advancements, Technologies 11 (2) (2023) 40.
[71] A. AlShibli, H. Mathkour, A shallow convolutional learning network for classification of cancers based on copy number variations, Sensors 19 (19) (2019) 4207.
[72] M. Amiri, R. Brooks, H. Rivaz, Fine-tuning U-Net for ultrasound image segmentation: different layers, different outcomes, IEEE Trans. Ultrason. Ferroelectr. Freq. Control 67 (12) (2020) 2510–2518.
[73] B. Chen, Composite optical scattering, 2025, URL https://github.com/BinChenOPEN/Composite_Optical_Scattering.